Beam Former Development for the NASA Hurricane Imaging Radiometer

Glenn D. Hopkins[1], James R. Skala[1], Daniel L. Revier[1], Mark W. James[2], David E. Simmons[3], Christopher S. Ruf[4], M.C. Bailey[5]
[1] Georgia Tech Research Institute, Georgia Institute of Technology, glenn.hopkins@gtri.gatech.edu
[2] NASA Marshall Space Flight Center, mark.w.james@nasa.gov
[3] University of Alabama in Huntsville, david.e.simmons@nasa.gov
[4] Space Physics Research Laboratory, University of Michigan, cruf@umich.edu
[5] Applied EM, Inc., m.c.bailey@cox.net

***Abstract*—The Hurricane Imaging Radiometer (HIRAD) is an airborne passive microwave synthetic aperture radiometer designed to provide high resolution, wide swath imagery of surface wind speed in tropical cyclones from a low profile planar array antenna. This paper will present the array radiometer system concept and summarize its development, including multiple flight tests on NASA's Genesis and Rapid Intensification Processes (GRIP, 2010) and Hurricane and Severe Storm Sentinel (HS3, 2012) campaigns. The paper will focus on the design goals, trades, and approach for the array antenna along-track beam former. The paper presents details of the beam former design, implementation, integration approach, and measured performance. The paper concludes with a description of planned improvements for the next generation dual-polarized HIRAD antenna and the resulting impacts on the beam former design and integration.**

***Index Terms*—**Tropical Cyclone, Imager, Aperture Synthesis Microwave Radiometer, Thinned Array Antenna, Analog Array Beam Former

TABLE OF CONTENTS

1. INTRODUCTION

The Hurricane Imaging Radiometer (HIRAD) [1] is an airborne passive microwave synthetic aperture radiometer designed to provide high resolution, wide swath imagery of surface wind speed in tropical cyclones from a low profile planar array antenna. Section 2. presents the array radiometer system concept and summarizes its development, including multiple flight tests on NASA's Genesis and Rapid Intensification Processes (GRIP, 2010) and Hurricane and Severe Storm Sentinel (HS3, 2012) campaigns. The paper focuses on the design and hardware development for the array antenna along-track beam former. This circuit is a passive 16-channel combiner, operating over 4 – 7 GHz and employing an amplitude taper for array antenna sidelobe reduction. Section 3 presents the architecture developed for the beam former. Section 4 presents details of the design of the individual combiners and their integration using a Transmission Line Method (TLM) circuit simulator. Section 5 presents the layout of the beam former and a comparison of measured results from a hardware prototype with modeled results using a commercial Finite Element Method (FEM) approach. Section 6 presents a comparison of the resulting antenna patterns from both hardware measurements as well as simulated patterns using both measured and modeled beam former data. The paper concludes in Section 7 with a summary and a description of planned improvements for the next generation dual-polarized HIRAD antenna and the resulting impacts on the beam former design and integration.

2. HURRICANE IMAGING RADIOMETER SYSTEM OBJECTIVES AND DEVELOPMENT

Airborne hurricane surveillance, conducted by the National Oceanic and Atmospheric Administration (NOAA) and the U.S. Air Force Reserve 53rd Weather Reconnaissance Squadron, is crucial to hurricane warnings issued by the National Hurricane Center. Flying specially equipped "Hurricane Hunter" aircraft, critical measurements are made of the hurricane eye location, the central pressure, and the maximum sustained (1-min average) surface wind speed. Of these, the surface wind speed is of greatest importance because this is the determining factor in the Saffir–Simpson hurricane scale commonly known as the hurricane category.

978-1-4799-5380-6/15/$31.00 ©2015 IEEE

One passive sensing approach measures 'emissivity' or noise temperature emitted from ocean surface foam coverage (a function of wind speed) and intervening rain. At C-band microwave frequencies (4-8 GHz), wind-driven foam coverage is nearly invariant with frequency while at the same time rainfall emissivity is a strong function of frequency. These physical characteristics allow two geophysical variables (wind speed and rain rate) to be derived from emissivity measurements at 4-6 discrete C-band frequencies, which is an 'over-determined', 'least-squares' problem solvable with conventional mathematical techniques. Surface wind speed and rain rate retrievals are derived from empirical correlation of measured emissivity at operating incidence angles with co-located GPS dropsonde surface wind observations and accepted functional relations for rain attenuation and wind-induced emissivity vs frequency.

For the past two decades, the airborne Stepped Frequency Microwave Radiometer (SFMR) has provided real-time measurements of surface wind speed and rain rate in hurricanes [2]. These measurements are crucial because SFMR is the only remote sensor that is capable of providing continuous measurements of surface wind speeds up to and including Category-5 hurricane conditions. However, there is one disadvantage of SFMR, which is the very narrow measurement swath directly beneath the aircraft. HIRAD has the potential to be the next generation replacement for the SFMR. HIRAD will improve airborne surveillance by imaging surface wind speed and rain rate over a wide swath, which is approximately equal to three times the aircraft altitude. Unlike SFMR's narrow swath, the HIRAD uses synthetic aperture thinned array radiometry technology to create a 1-D microwave imager that synthesizes horizontally polarized brightness temperature, Tb, images cross-track and provides real-aperture imaging alongtrack. A comparison of the SFMR and HIRAD coverage is shown in Figure 1.

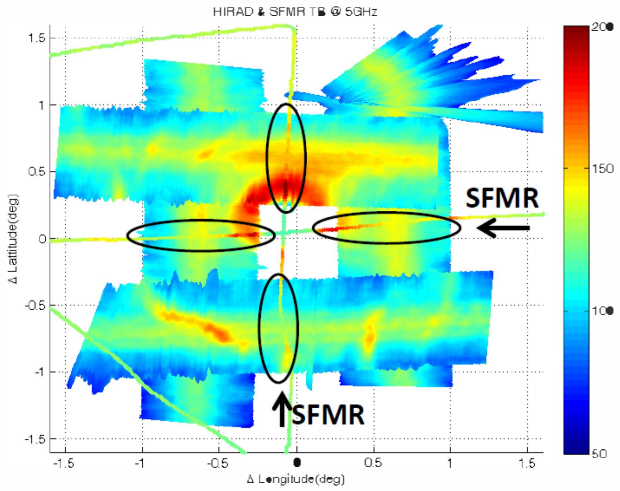

Figure 1. Comparison of measured SFMR (narrow) and HIRAD (wide) radiometer swaths over Hurricane Earl in 2010 [from Miller, ref 3].

The key to HIRAD's improved performance is its ability to operate as a Fourier synthesis imager at four discrete frequencies (4, 5, 6, and 6.6 GHz) that cover approximately the same C-band octave as the SFMR. The HIRAD aircraft instrument, shown in an operational concept in Figure 2, has been developed over the past 4 years under a NASA Marshall Space Flight Center (MSFC) led collaboration with NOAA's Atlantic Oceanographic and Meteorological Laboratory Hurricane Research Division, the Central Florida Remote Sensing Laboratory (CFRSL) at the University of Central Florida and the Space Physics Research Laboratory of the University of Michigan. The Georgia Tech Research Institute (GTRI) contributed by developing the along-track array beam former. GTRI also assisted in the development of the manufacturing process with the array fabricator to successfully integrate the multilayer radiator and beam former assembly. The analog beam former is responsible for beam formation in the along-track direction and is the subject of this paper. Figure 3 shows the block diagram of the HIRAD sensor and the location of the prototype along-track beam former.

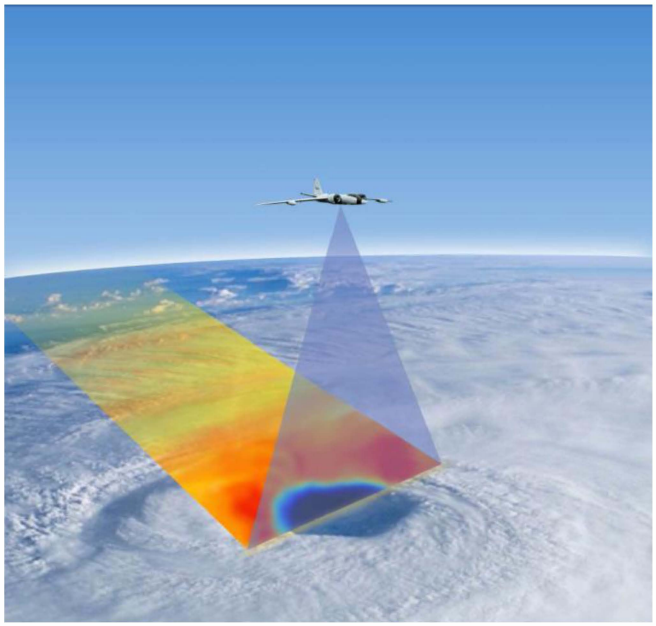

Figure 2. Operational concept of the HIRAD system as employed on a high altitude aircraft, mapping the wind speed and rain rate of a tropical storm [from Miller, ref 3].

The HIRAD system was developed prototyped and integrated by NASA MSFC. Its first operational flights on high-altitude aircraft were over hurricanes Earl and Karl during NASA's GRIP (Genesis and Rapid Intensification Processes) campaign in August – September of 2010 on NASA's WB-57 airframe. HIRAD also flew during NASA's HS3 (Hurricane and Severe Storm Sentinel) campaign on the Global Hawk in November 2012. As this paper is being written in October 2014, HIRAD is once again flying on the WB-57, taking measurements on Hurricane Gonzalo.

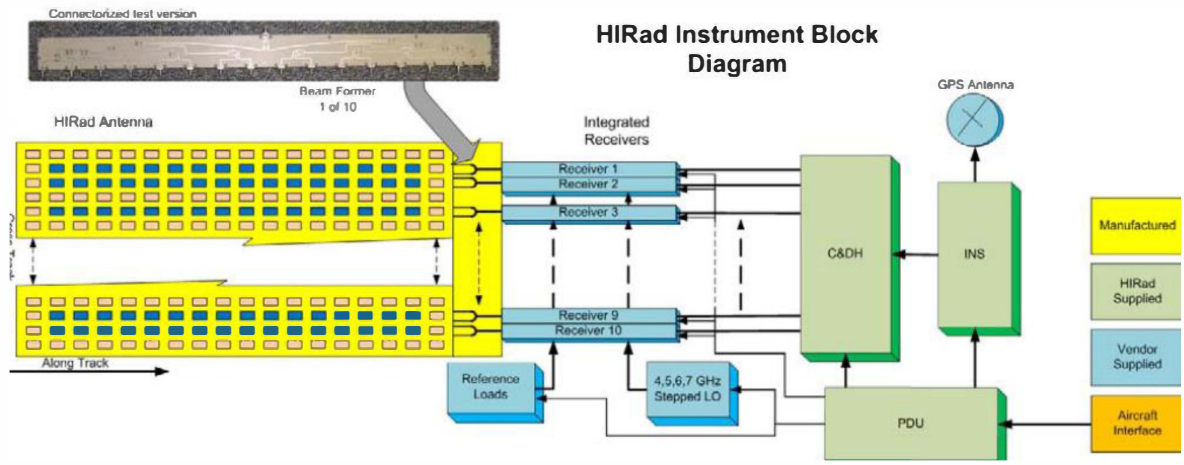

Figure 3. Block diagram of the HIRAD instrument and the location of the along-track beam former [Fenigstein ref 4].

Figure 4. HIRAD installed in the NASA WB-57 bay (above) and the flight, science, and ground crews with the WB-57 (below).

Figure 5. The NASA Global Hawk (above) and a closeup of its HIRAD installation (below).

Fig. 4 shows the HIRAD flight array on the NASA WB-57 pallet that was flown during 2010. Figure 5 shows the HIRAD flight array on the NASA Global Hawk that was flown during 2012. For further information regarding the HIRAD system, its theory, and data collected from numerous test flights during the period from 2010-2014, the authors refer the reader to either the HIRAD website [1] or additional prior publications [3-8].

3. Beam Former Circuit Architecture

The HIRAD along-track beam former sums the received signals from 16 multi-banded microstrip stacked patch radiators in columns which are oriented in the direction of forward flight, or the along-track direction. It was originally intended to support four separate narrow frequency bands centered around 4, 5, 6, and 7 GHz. Later in the program, the uppermost band was lowered to 6.6 GHz; however, as the beam former was designed to support the contiguous band from 4 to 7, no modifications were necessary to the design. The design of the radiators and of the multi-channel radiometer array are presented in Bailey [5]. The beam former was constructed in single layer microstrip and was

directly integrated with the four-substrate, multilayer patch radiator – resulting in a 6-layer, 5-substrate stackup.

Because of thermal cycling concerns and the desire for low transmission loss, Rogers Corporation 6002 and 6202PR substrates were selected. These materials have Coefficients of Thermal Expansion (CTE) that are closely matched to copper, the primary metallization used in the circuit traces and plated-through-holes. The 6002 material has a relative permittivity (ε_r) of 2.94 and a loss tangent ($\tan(\delta)$) of 0.012. Using a 0.020 inch thickness resulted in a 50Ω trace width of approximately 0.0493 inch. This substrate thickness and relatively wide trace width reduces transmission loss as compared to narrower traces, and facilitates the thinner traces for the higher impedance lines required in the distributed combiner circuits for the beam former. The microstrip circuit was contained in a metal enclosure; however, the height of the lid was such that it did not significantly influence the beam former circuit layout.

Performance goals for the circuit included: amplitude taper to achieve a first sidelobe level of -25 dB, reflection coefficient at any port of -17.8 dB or better, transmission coefficient from radiator port to radiator port of -20 dB or better, and frequency coverage of 3.9 – 7.1 GHz.

To achieve the along-track array sidelobe level goals, a Taylor amplitude taper was employed [9]. With the goal of achieving a -25 dB first sidelobe, a taper to achieve a -27 dB first sidelobe with a Taylor nbar parameter of 3 was used. A -3dB combiner was used to feed the two 1:8 symmetric halves of the 1:16 beamformer, therefore only half of the calculated amplitude distribution is shown in Figure 6.

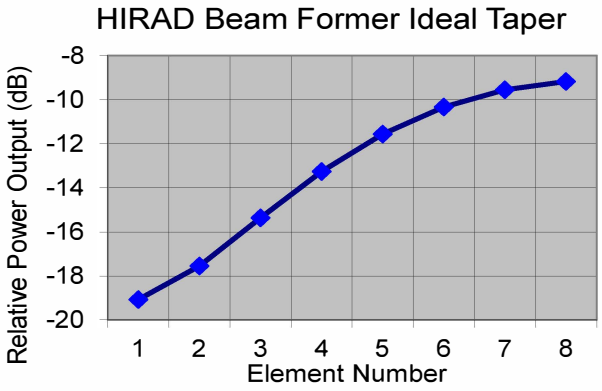

Figure 6. The ideal amplitude at each radiator element in one half of the HIRAD beam former.

To support the full instantaneous bandwidth goal of almost an octave, a parallel corporate feed network was required. Use of a traditional binary network would have required unfeasible differential amplitude at the second combiner into the network. This is because the outer-most elements (1-4 in Figure 6) have a significantly lower total power as compared to the inner-most elements (5-8). Figure 7 presents such a binary beam former, identifying the largest differential amplitude required.

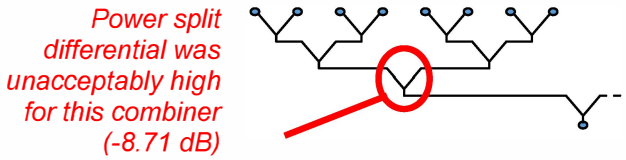

Figure 7. Binary beam former concept that would have resulted in unacceptably high differential amplitude at one of the combiners.

The beam former power combiners were fundamentally based on the equal power combiner approach of Wilkinson [10], implemented in microstrip. To achieve wider frequency bandwidth and unequal split, the combiners followed the design approach of Parad and Moynihan [11]. This approach uses multiple stages of impedance transformation to achieve higher bandwidth. To achieve the unequal power split, lower and higher impedances are used in the transformers on the two sides of a single combiner. Depending upon the number of transformer stages and the magnitude of the desired unequal power split, the highest-impedance trace required to achieve these goals can become prohibitively narrow – so narrow that it is impractical to manufacture because of tolerance issues using conventional printed circuit fabrication techniques. The goal of the beam former architecture selection is to develop a parallel approach where the line-lengths from each radiator to the central connector are still all the same, yet the maximum power differential in any single combiner is preferably between 0 and -3 dB. GTRI developed the power split architecture shown in Figure 8, which achieved the goals of the power division for the Taylor taper, yet required a maximum differential amplitude from any single combiner of only -1.847 dB. The division architecture used in the HIRAD sensor is shown in Figure 8. The eight individual combiners required were named letter A through H.

4. Unequal Combiner Designs and TLM Models

The HIRAD beam former was designed using a Transmission Line Method code named the Advanced Design System (ADS), commercially available from Keysight Technologies (formerly Agilent Technologies) [12]. The first step was to assess the number of stages required for each of the individual power combiners. Initial models determined that two-stage combiners would not have provided enough bandwidth margin, therefore three-stage combiners were required. To reduce the combiner

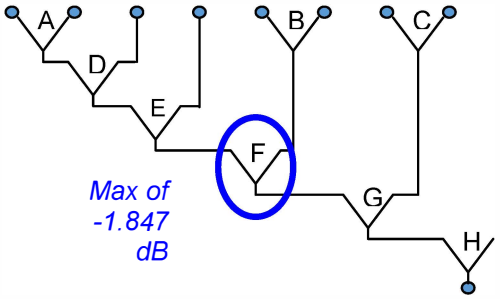

Figure 8. Power combining architecture of the HIRAD beam former.

area footprint, it was decided to use only the isolation resistors with the inner two stages. The goals for the optimized designs of the combiners A through H were to achieve: the desired power split, equal phase on the two output legs, low reflection coefficient on every port, and good isolation between the two output legs. Figures 9 through 11 present the layout and predicted performance for an individual combiner design, in this case combiner A, which had a targeted differential amplitude of -1.518 dB. The layout and performance of the other combiners B through H were similar.

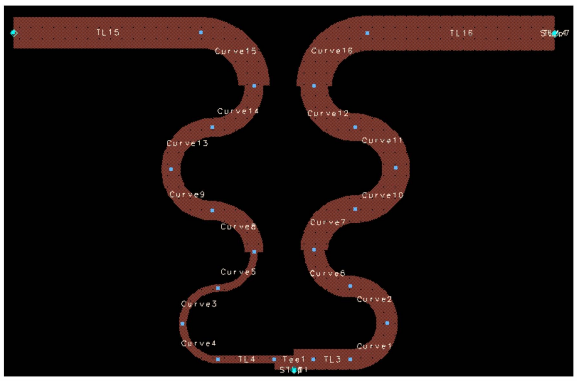

Figure 9. Artwork layout for combiner A.

5. Prototype Layout and Measured and FEM Results

The HIRAD array only synthesizes beams in the cross-track direction, and the radiator spacing in that direction was 0.9 inch. The radiator spacing in the along-track direction was 1.5 inches. Because of the thinned array topology, the beamformer was allowed to occupy up to 1.8 inches in the cross-track direction. The beam former circuit was assembled and linelengths were optimized, again using ADS. The surface mount SMA to microstrip transition was modeled using a Finite Element Method (FEM) tool, the High Frequency Structure Simulator (HFSS), commercially available from ANSYS [13]. The data from the connector transition simulation was included in ADS as a two-port S-

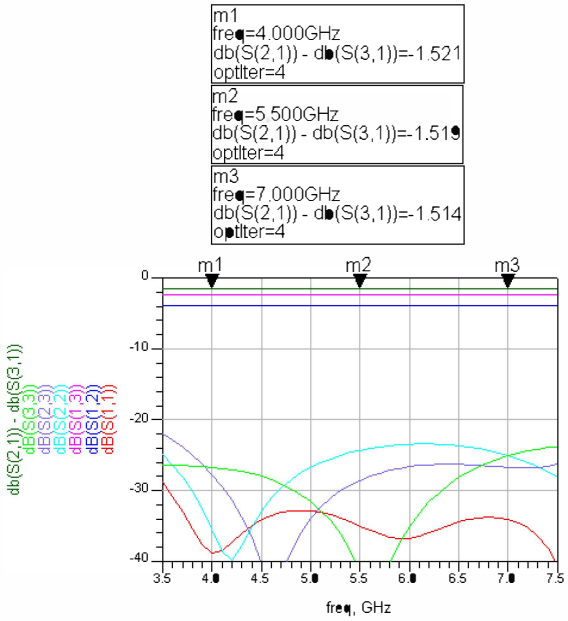

Figure 10. S-parameter amplitude for combiner A

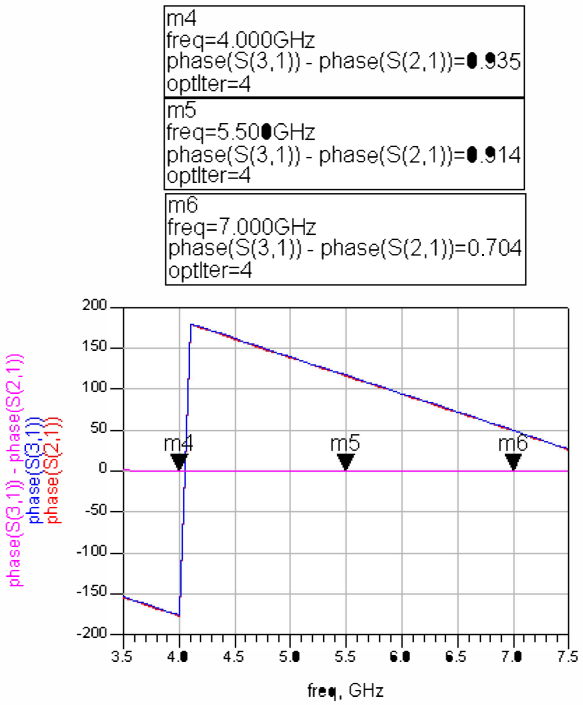

Figure 11. S-parameter phase for combiner A.

parameter block. The final circuit had a board size of 1.8 inches by just under 24 inches.

To verify performance independent from the array assembly, the beam former was prototyped with connectors at every port, and its performance was measured. A closeup of one end of the prototyped beam former is presented in Figure 12. This photograph includes combiners A, B, and D – G. The shielding was included to minimize cross-talk between transmission line runs as much as possible. Although the shielded microstrip layout appears similar to

grounded coplanar waveguide, the gap between the microstrip trace and the ground structure is wide and the resulting transmission mode is that of microstrip.

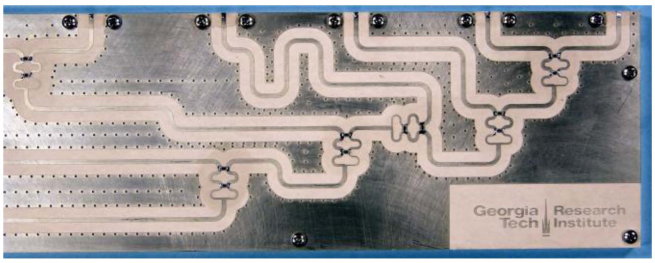

Figure 12. A photograph of a portion of the prototyped HIRAD along-track beam former.

The measured and predicted data compared acceptably with one notable exception - the transmission phases of the 16 outputs. Figure 13 presents a comparison between the ideal Taylor amplitude for a lossless beam former (red) with the measured performance at four different frequencies. The amplitude taper compared very well and had an average transmission loss over frequency and radiator port of approximately -2 dB.

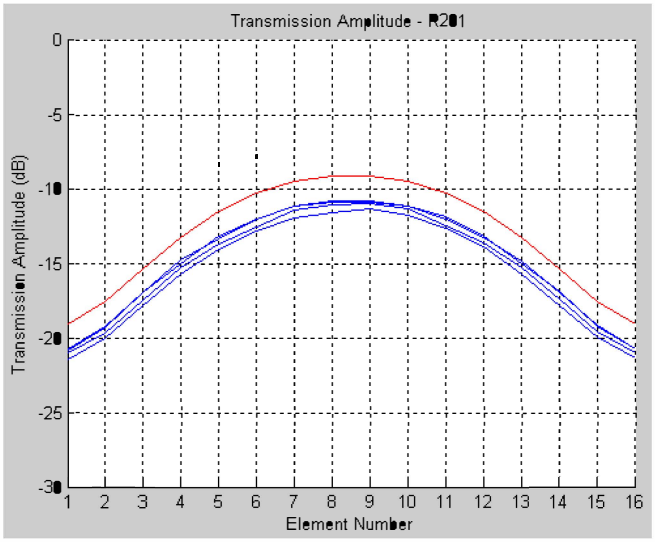

Figure 13. Comparison of the ideal, lossless Taylor amplitude (red) with that measured from the prototype at four frequencies of 4, 5, 6, and 7 GHz (all blue).

Figure 14 presents the predicted receiver port reflection coefficient and transmission coefficients versus frequency. Figure 15 presents the measured single receiver port reflection coefficient from the prototype. Figure 16 presents the predicted 15 nearest neighbor radiator port coupling coefficients, all of which were better than -20 dB. Figure 17 presents the measured 15 nearest neighbor radiator port couplings, all of which were better than -17 dB.

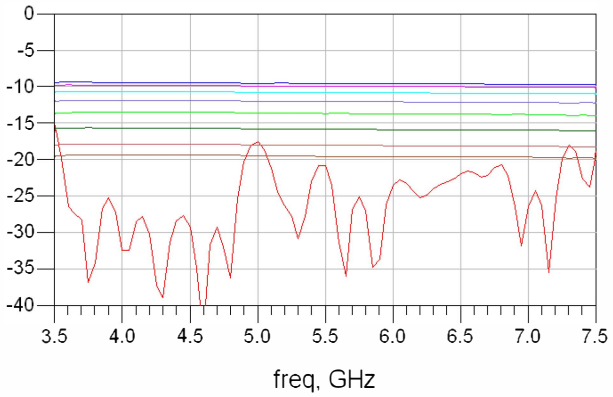

Figure 14. Predicted receiver port reflection (lower fluctuating trace) and radiator port transmission (upper nearly straight-line) coefficient amplitudes.

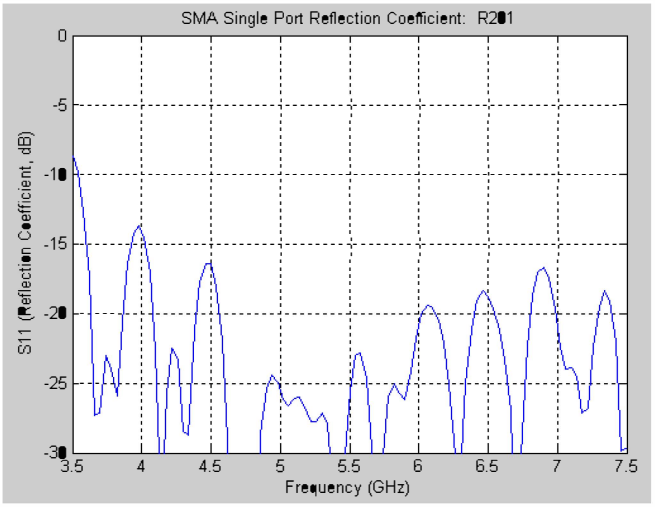

Figure 15. Measured reflection coefficient from the single receiver port of the HIRAD beam former.

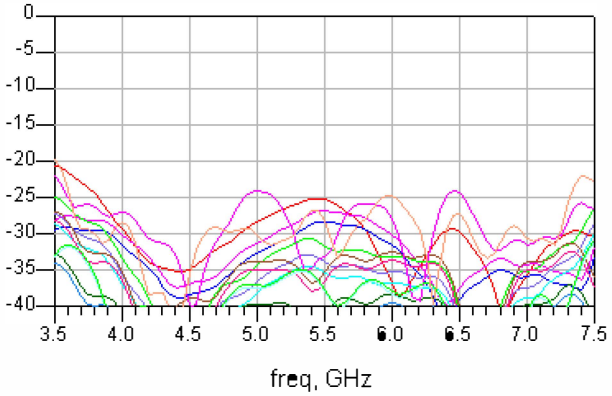

Figure 16. Predicted nearest neighbor coupling between radiator ports

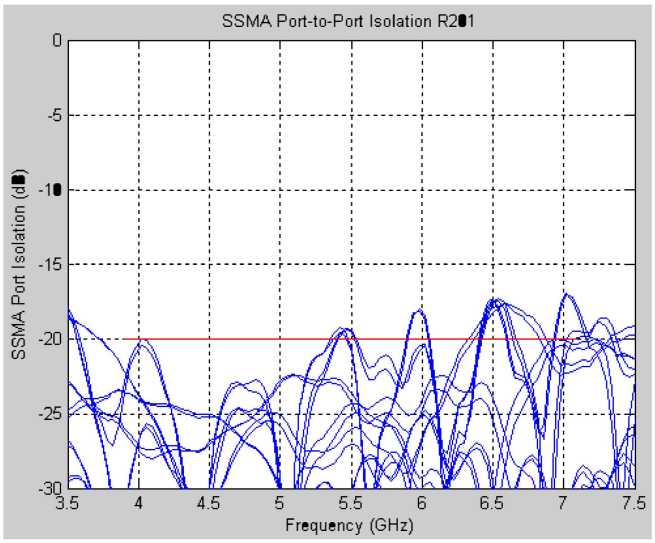

Figure 17. Measured nearest neighbor coupling between radiator ports.

The performance parameter that most deviated between predicted and measured was the transmission phase across the 16 radiator ports. Figure 18 presents the predicted phase, which were fairly flat ramps. Figure 19 presents the measured phases. The primary difference to note between Figures 18 and 19 are the maximum spread of difference between the two as the predicted phase had a maximum deviation across ports for any one frequency of less than 4° while the same measured data had a maximum deviation of approximately 50°. Figure 20 presents the same measured data as Figure 19, except that the horizontal axis is now the element location and the different traces are for frequencies of 4, 5, 6, and 7 GHz. Note that the desired flat phase radiates from the array as a defocused, curved phase front.

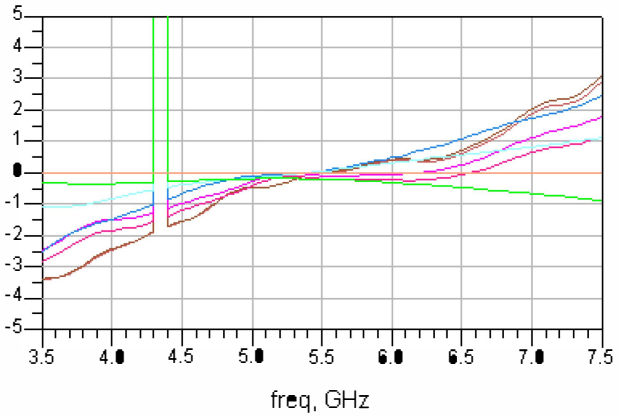

Figure 18. Predicted transmission phase at the 16 radiator ports.

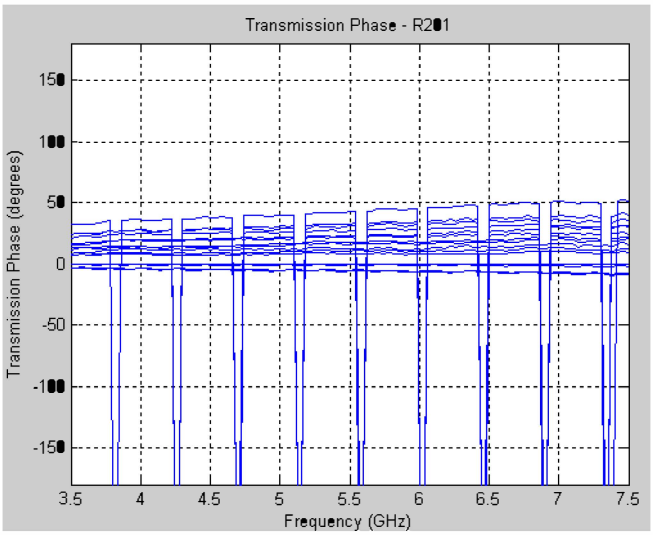

Figure 19. Measured transmission phase at the 16 radiator ports.

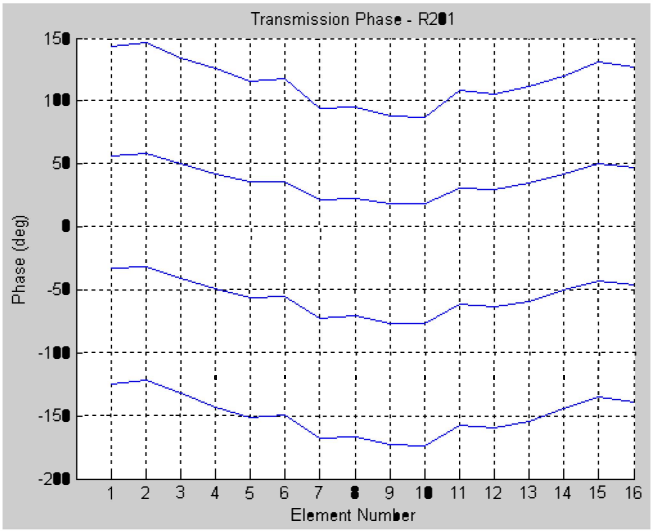

Figure 20. Measured transmission phase at the 16 element radiator ports with the element number as the horizontal scale.

The discrepancy between the measured and modeled phase at the radiator ports results in a defocusing of the plane wave and an increase in the array along-track sidelobe levels. The cause of the difference is believed to be coupling between the traces within each combiner, which is not taken into consideration in the TLM modeling approach. To verify this assumption, GTRI modeled the combiner using the FEM code, HFSS. To minimize model computational size, the beam former geometry was divided into two portions: a central equal-power combiner, and the outer combiners that contain the desired amplitude taper and suspected phase taper error. The field visualizations of the two HFSS model segments are shown in Figure 21. The results of the two portions of the model were recombined in Ansys Designer to give performance of the complete beam former.

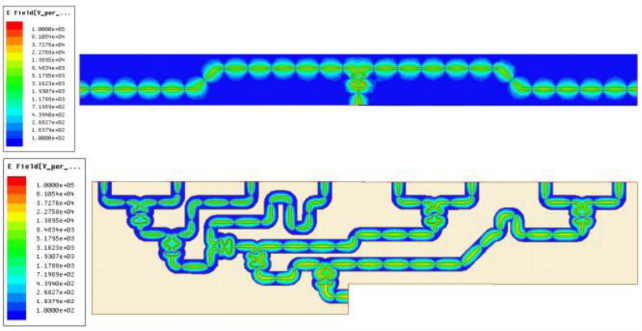

Figure 21. HFSS-generated models of the beam former equal-power split central section (upper) and one side of the beam former with the amplitude taper.

The HFSS modeling effort confirmed that the beam former amplitude taper and loss were similar to both predicted and measured, and that the phase at the radiator ports correlated well with the measured phase but not with the TLM predicted phase. The HFSS-predicted transmission amplitude and phase versus output port at frequencies of 5, 6, and 6.6 GHz are presented in Figure 22. Note that the phase values of Figure 22 are normalized to the total phase at port 8 for all frequencies. For comparison, refer to the measured amplitude in Figure 13 and the measured phase in Figure 20. The phase curvature apparent in the measured data in Figure 20 and in the HFSS modeled data in Figure 22 results in pattern defocusing and higher sidelobes which will be discussed in Section 6.

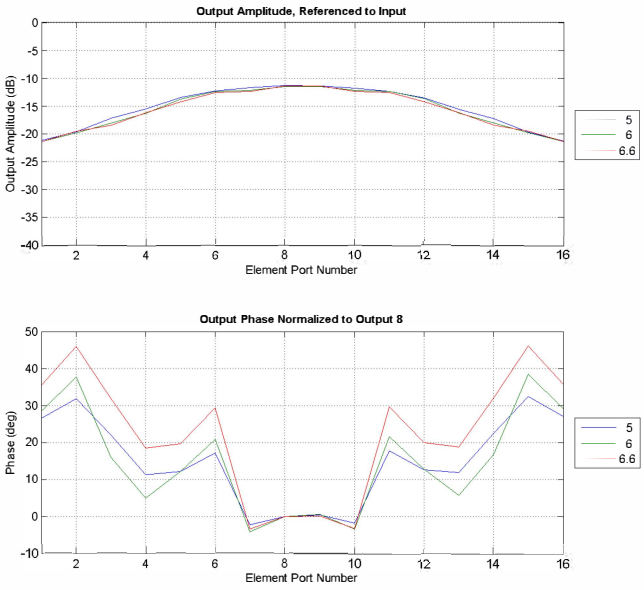

Figure 22. HFSS-predicted amplitude and phase at the 16 radiator ports.

The HFSS modeling effort corroborated the measured performance of acceptable amplitude and unacceptable phase performance of the prototyped beam former. This information was used in the improvements implemented in the flight design.

6. Simulated Antenna Patterns Based on the Prototype Beam Former

Figures 27-29 present predicted patterns for the along track linear array at 5, 6, and 6.6 GHz where the HFSS-modeled beam former data was used with an ideal linear array with radiating elements having a cos(θ) pattern. Similarly, Figures 30-33 present the predicted patterns for 4, 5, 6, and 6.6 GHz where the measured prototype beam former data was used with an ideal linear array with radiating elements having a cos(θ) pattern.

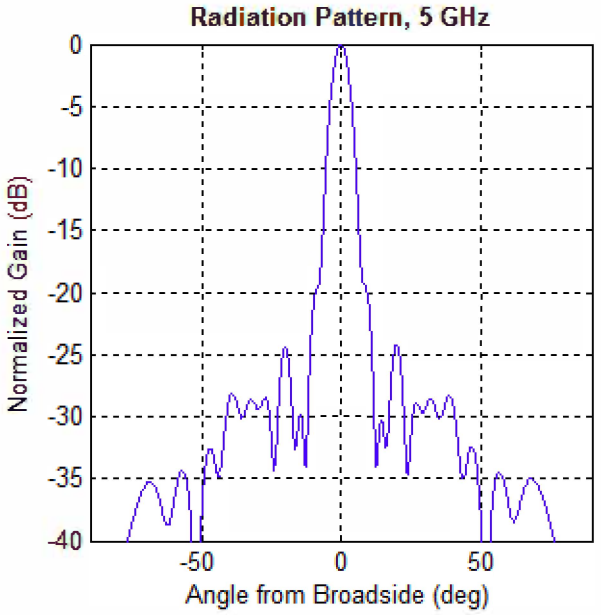

Figure 27. Predicted along-track pattern at 5 GHz based on beam former data from HFSS using a cos(θ) element pattern

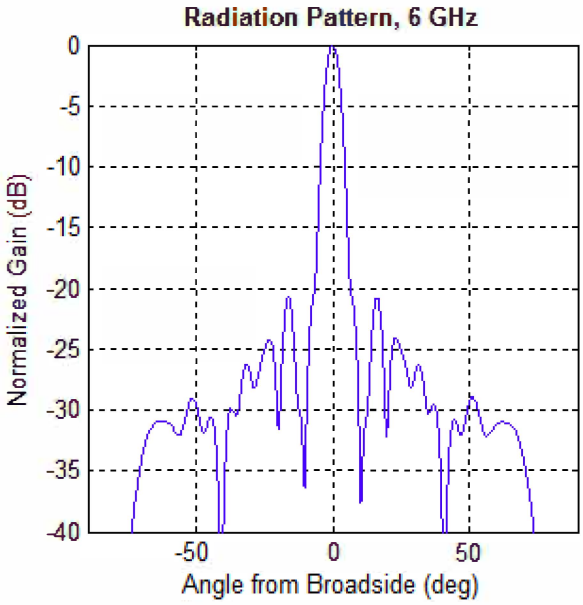

Figure 28. Predicted along-track pattern at 6 GHz based on beam former data from HFSS using a cos(θ) element pattern

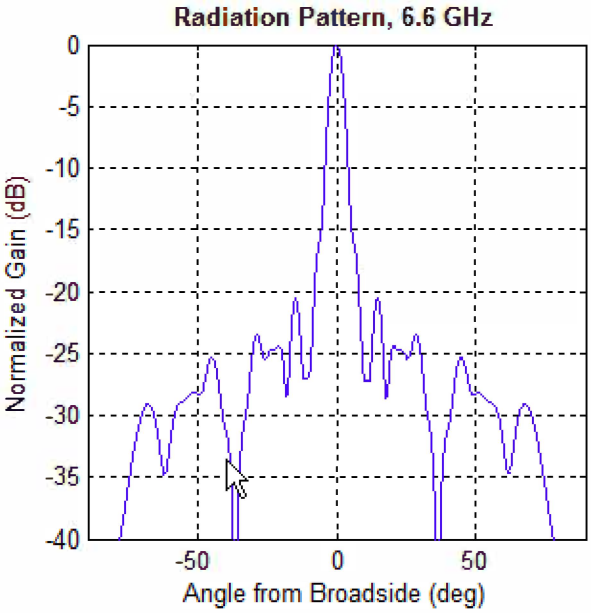

Figure 29. Predicted along-track pattern at 6.6 GHz based on beam former data from HFSS using a cos(θ) element pattern

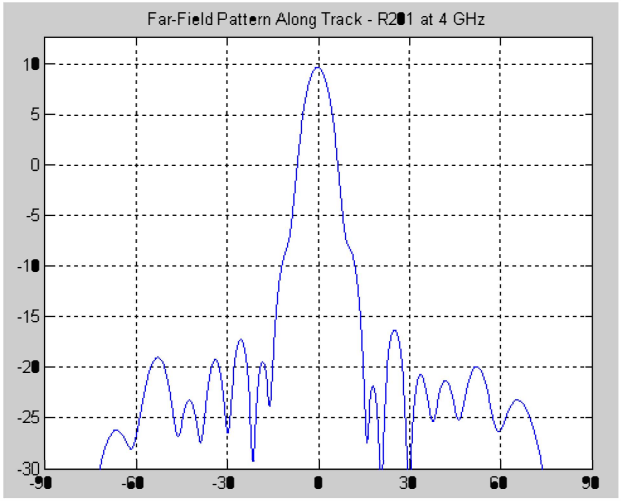

Figure 30. Predicted along-track pattern at 4 GHz, based on measured beam former data using a cos(θ) element pattern

.

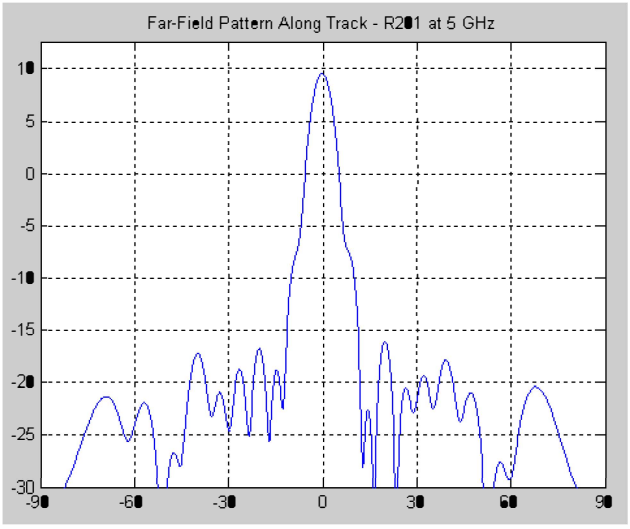

Figure 31. Predicted along-track pattern at 5 GHz, based on measured beam former data using a cos(θ) element pattern.

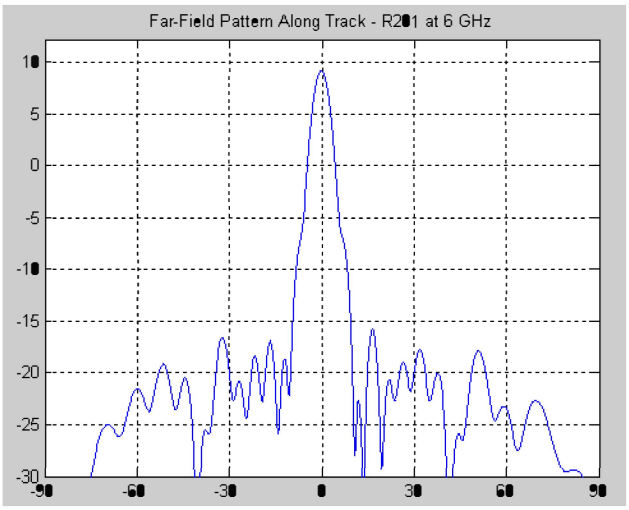

Figure 32. Predicted along-track pattern at 6 GHz, based on measured beam former data using a cos(θ) element pattern.

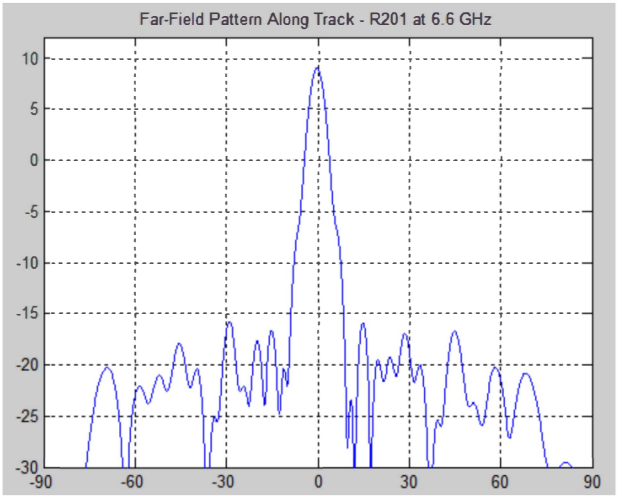

Figure 33. Predicted along-track pattern at 6.6 GHz, based on measured beam former data using a cos(θ) element pattern.

7. Beam Former Flight Design and Pattern Test Data

Improvements were made to the beam formers designed for integration with the multilayer array and flight testing of the entire HIRAD system. The improvements included adjustments to flatten the phase curvature that resulted in pattern defocusing as well as layout of a different isolation fence that included keep-outs for the film resistor terminations of radiators that were not connected to any of the beam formers. A prototype version of the final flight beam former was not constructed and tested separately. The panel layouts for the subarray and radiator termination layers were completed by GTRI. The array was constructed in two halves, which had different layouts because of the sparse interferometer design. Figure 34 presents the top-layer artwork for the entire array, showing the location of the ten along-track beam formers. Eleven beam formers were integrated, however the additional central one was used only to facilitate beam pointing alignment in range pattern testing.

Antenna patterns for the completed array were measured for the ten along-track linear arrays in MSFC's indoor anechoic chamber, as shown in Figure 35. Figures 36 – 39 present measured radiometer patterns of the integrated system using a noise diode as the illumination source. The pattern noise floor of this data is essentially the ambient thermal temperature of the test facility.

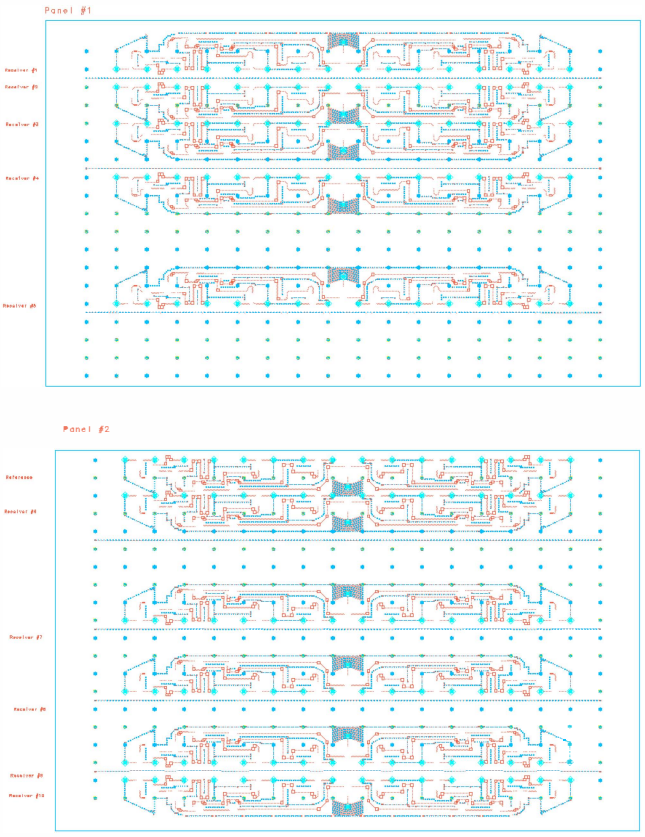

Figure 34. The beam former artwork of both of the HIRAD array panels

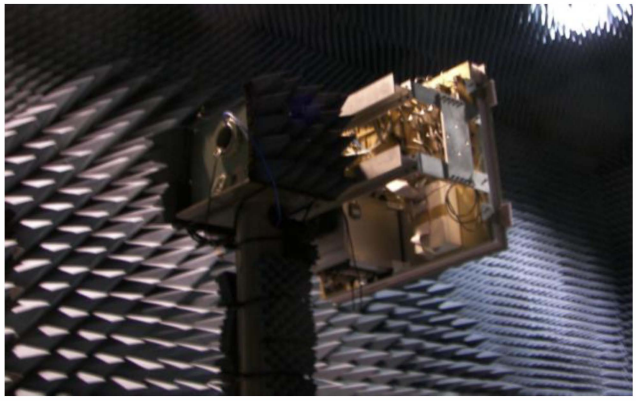

Figure 35. A photograph of the HIRAD system during measurements at the NASA MSFC Facility

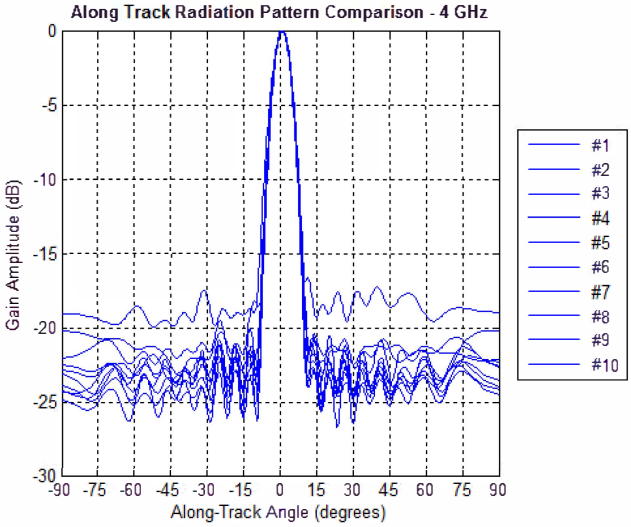

Figure 36. Measured HIRAD along-track radiometer pattern at 4 GHz

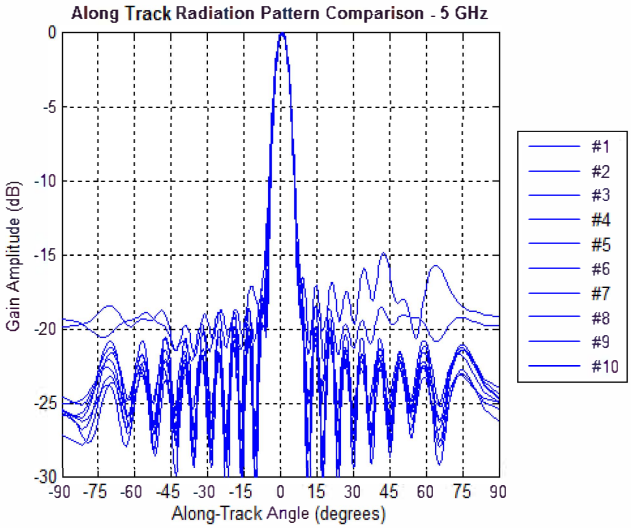

Figure 37. Measured HIRAD along-track radiometer pattern at 5 GHz

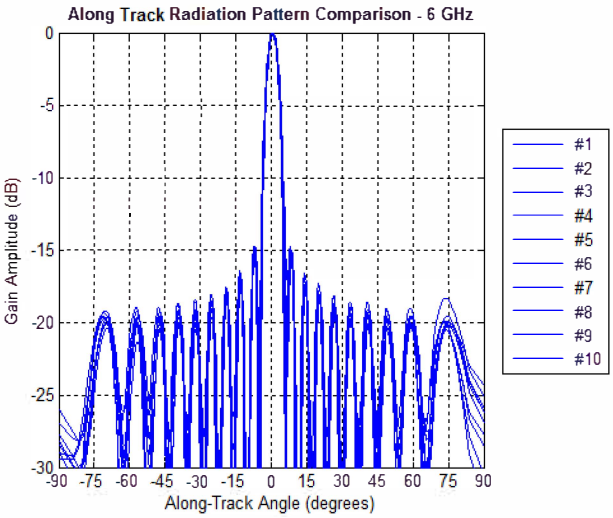

Figure 38. Measured HIRAD along-track radiometer pattern at 6 GHz

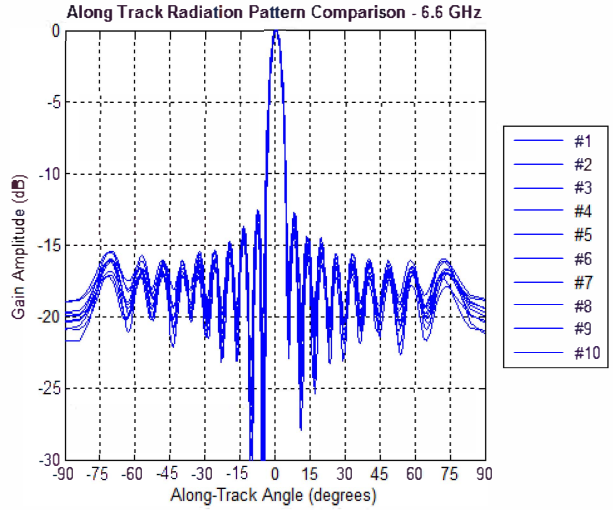

Figure 39. Measured HIRAD along-track radiometer pattern at 6.6 GHz

8. Summary and Future Work

This paper presented the design details and process used in the development of the along-track beam formers successfully integrated and flight tested with the Hurricane Imaging Radiometer. Trades in the architecture development, the design approach using the TLM method, and verification using further FEM modeling and measurements were presented.

A second iteration of the HIRAD system has been proposed for development. Key improvements will include a wide-band dual-polarized radiator and dual beam formers for each linear array, one for each orthogonal linear polarization.

Acknowledgements

This work was supported by the HIRAD Project of the NASA Marshall Space Flight Center. GTRI gratefully acknowledges the contributions by researchers at NASA MSFC, NOAA, University of Michigan, University of Central Florida, and others for the content contained herein regarding the HIRAD system.

REFERENCES

[1] More information on the HIRAD system and its development can be found at the NASA HIRAD website at: http://hirad.nsstc.nasa.gov

[2] E. W. Uhlhorn, P. G. Black, J. L. Franklin, M. Goodberlet, J. Carswell, and A. S. Goldstein, "Hurricane surface wind measurements from an operational stepped frequency microwave radiometer," *Monthly Weather Rev.*, vol. 135, no. 9, pp. 3070–3085, Sep. 2007.

[3] Miller, T. L., M. W. James, W. L. Jones, C. S. Ruf, E. W. Uhlhorn, C. D. Buckley, S. Biswas, G. Shah, and R. E. Hood, "Development and Validation of a Capability for Wide-Swath Storm Observations of Ocean Surface Wind Speed," 65th Interdepartmental Hurricane Conference, Feb-Mar 2011, Miami.

[4] Fenigstein, D., C. Ruf, M. James, D. Simmons, T. Miller, C. Buckley, "Analysis Of Anechoic Chamber Testing Of The Hurricane Imaging Radiometer," IGARSS 2010, July, Honolulu.

[5] Bailey, M. C., Ruba Amarin, James Johnson, Paul Nelson, Mark James, David Simmons, Christopher Ruf, Linwood Jones and Xun Gong, "Multi-Frequency Synthetic Thinned Array Antenna for the Hurricane Imaging Radiometer", IEEE Trans. Ant. & Prop., vol – 58, no. 8, pp. 2562-2570, Aug 2010.

[6] Ruf, C., R. Amarin, M.C. Bailey, B. Lim, R. Hood, M. James, J. Johnson, L. Jones, V. Rohwedder and K. Stephens, "The Hurricane Imaging Radiometer – An Octave Bandwidth Synthetic Thinned Array Radiometer," Proc. 2007 IEEE International Geoscience and Remote Sensing Symposium, Barcelona, SPAIN, 23-27 July, 2007.

[7] Jones, Linwood, Timothy Miller, Robert Atlas, M. C. Bailey, Peter Black, Salem El-Nimri, Robbie Hood, Mark James, James Johnson, Christopher Ruf, and Eric Uhlhorn, "Surface Wind Vector and Rain Rate Observation Capability of the Future Airborne Hurricane Imaging Radiometer (HIRAD)", 2009 NASA Ocean Vector Wind Sci Team Meeting, May 18-20, 2009, Boulder, CO.

[8] Miller, T. L., M. W. James, J. B. Roberts, S. K. Biswas, D. Cecil, W. L. Jones, J. Johnson, S. Farrar, S. Sahawneh, C. S. Ruf, M. Morris, E. W. Uhlhorn, and P. G. Black, "The Hurricane Imaging Radiometer: Present and Future," IGARSS 2013, Melbourne Australia, July 21-26, 2013.

[9] Taylor, T. T., "Design of Line Source Antennas for Narrow Beamwidth and Low Sidelobes," IEEE Trans. Ant. & Prop., January, 1955.

[10] Wilkinson, E. J., "An N-Way Hybrid Power Combiner," IRE Trans. On Microwave Theory & Techniques, Vol. 8, No. 1, pp. 116-118, January, 1960.

[11] Parad, L. I., and R. L. Moynihan, "Split-Tee Power Combiner," IEEE Trans. On Microwave Theory & Techniques, Vol. 13, No. 1, pp. 91-95, January, 1965.

[12] Information regarding the Advanced Design System software can be found at: http://www.keysight.com/find/eesof

[13] Information regarding the High Frequency Structure Simulator software can be found at http://www.ansys.com/Products/Simulation+Technology/Electronics/Signal+Integrity/ANSYS+HFSS

BIOGRAPHY

Glenn D. Hopkins *received a B.E.E. and M.S.E.E. from the Georgia Institute of Technology in 1987 and 1991. He has been with the Georgia Tech Research Institute for more than 27 years. As the Chief Antenna Systems Engineer of the Sensors and Electromagnetic Applications Laboratory, he develops and leads a range of programs involving innovation and development of advanced array antennas. Mr. Hopkins was the recipient of the 2010 GTRI Innovative Research Award. He is a Senior Member and is active with the IEEE Antennas and Propagation and Microwave Theory and Techniques Societies and has 78 technical publications. Mr. Hopkins has been awarded three U.S. Patents and currently teaches in ten Georgia Tech Professional Education courses.*

James R. Skala *received the B.S.E.E. from the University of Nebraska in 2002 and M.S. Physics from the University of Washington in 2009. He has been employed at the Georgia Tech Research Institute since 2009. He is currently an electromagnetics and antennas analyst for the Sensors and Electromagnetic Applications Laboratory, regularly works in design of single and array antennas, and is an instructor in the Modeling and Simulation of Antennas professional education course. His prior experience includes antenna and microwave measurements, as well as analysis and test for aerospace lightning qualification and electromagnetic compatibility while working for Boeing.*

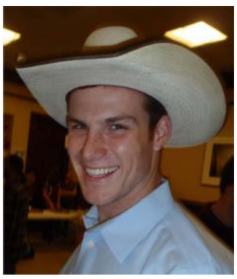

Daniel Revier *received the B.E.E. degree from Texas A&M in 2012 and is currently working on the M.S.E.E from the Georgia Institute of Technology in tandem with working for the Georgia Tech Research Institute as a research engineer. His primary roles at GTRI include leading testing in the electromagnetic anechoic chamber and supporting projects, focusing in fixed beam and phased array systems. His long-term goals include becoming an antenna, propagation and electromagnetic expert with a focus in utilizing additive manufacturing and rapid prototyping to facilitate the advancement of active and passive RF systems.*

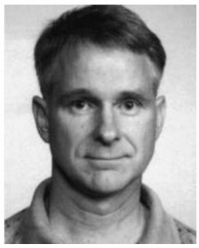

Mark W. James *received the B.S. degree in electrical engineering technology from Purdue University, West Lafayette, IN, in 1978 and the B.S. degree in electrical and computer engineering from the University of Michigan, Ann Arbor, in 1984. He is currently employed by NASA, Marshall Space Flight Center, Huntsville, AL, in the Engineering Directorate. He has worked previously at the Space Physics Research Laboratory, University of Michigan, Daedalus Enterprises, and Delco Electronics. He has coauthored in the areas of microwave and near-infrared remote sensing. He has been involved in the development of microwave radiometers, Near IR and visible spectrum airborne spectrometers, data acquisition systems and lightning detection sensors. Mr. James is a registered Professional Engineer in the State of Alabama. He has received numerous NASA awards including the Directors Commendation for technical excellence and Exceptional Service Award.*

David E. Simmons *received the B.S. degree in electrical engineering from Tennessee Technological University, Cookeville, in 1979. He is currently employed by the University of Alabama, Huntsville. He has previously worked for BAE Systems / MEVATEC, Jacobs/Sverdrup, Chrysler, GTE and Honeywell. He has served in various technical roles since graduation on commercial, DoD and NASA projects. He has designed and supported airborne passive radiometer system electronics, missile testing, flight experiments, automotive and telephony electronics testing and military communications equipment.*

Christopher S. Ruf *received the B.A. degree in physics from Reed College, Portland, OR, and the Ph.D. degree in electrical and computer engineering from the University of Massachusetts, Amherst. He is currently a Professor of atmospheric, oceanic, and space sciences and electrical engineering and computer science and Director of the Space Physics Research Laboratory, University of Michigan, Ann Arbor. He has worked previously at Intel Corporation, Hughes Space and Communication, the NASA Jet Propulsion Laboratory, and Penn State University. In 2000, he was a Guest Professor with the Technical University of Denmark, Lyngby. He has published in the areas of microwave radiometer satellite calibration, sensor and technology development, and*

atmospheric, oceanic, land surface and cryosphere geophysical retrieval algorithms. Dr. Ruf is a member of the American Geophysical Union (AGU), the American Meteorological Society (AMS), and Commission F of the Union Radio Scientifique Internationale. He has served on the Editorial Boards of the AGU Radio Science, the IEEE TRANSACTIONS ON GEOSCIENCE AND REMOTE SENSING (TGRS), and the AMS Journal of Atmospheric and Oceanic Technology. He is currently the Editor-in-Chief of the IEEE TRANSACTIONS ON GEOSCIENCE AND REMOTE SENSING. He has been the recipient of three NASA Certificates of Recognition and four NASA Group Achievement Awards, as well as the 1997 TGRS Prize Paper Award, the 1999 IEEE Resnik Technical Field Award, and the IGARSS 2006 Symposium Prize Paper Award.

M. C. Bailey *received the B.S. degree in electrical engineering from Mississippi State University, Starkville, in 1964, the M.S. degree in electrical engineering from University of Virginia, Charlottesville, in 1967, and the Ph.D. degree in electrical engineering from Virginia Polytechnic Institute and State University, Blacksburg, in 1973. He is currently employed part-time by Applied EM, Hampton, VA and also serves as a Technical Consultant for the University of Central Florida, Orlando. He previously worked for Research Triangle Institute, Hampton, VA after retiring from NASA, Langley Research Center, Hampton, VA in 2000 with 36 years of federal government employment as a research engineer. He was a Visiting Professor at the University of Mississippi, Oxford, during the 1978–79 academic year. He has authored or coauthored over 110 publications in the field of antennas and electromagnetics. He coauthored the section "Antennas and Wave Propagation" in the Electronics Engineers' Handbook (McGraw-Hill, 1982, 2nd ed), and coauthored the chapter "Radiometer Antennas" in the Antenna Engineering Handbook (McGraw-Hill, 1984, 2nd ed). Dr. Bailey has been the recipient of 27 NASA awards for recognition of technical accomplishments, including the NASA Medal for Exceptional Scientific Achievement.*